Advanced Fiber Materials (2021) 3:26–37
https://doi.org/10.1007/s42765-020-00059-3

RESEARCH ARTICLE

Multifunctional Fibroblasts Enhanced via Thermal and Freeze-Drying Post-treatments of Aligned Electrospun Nanofiber Membranes

Ya Li[1,2] · Qian Shen[3] · Jing Shen[2] · Xinbo Ding[1] · Tao Liu[1] · Jihuan He[2] · Chengyan Zhu[1] · Ding Zhao[4] · Jiadeng Zhu[5]

Received: 28 June 2020 / Accepted: 17 December 2020 / Published online: 12 January 2021

Abstract

Parallel fibrous scaffolds play a critical role in controlling the morphology of cells to be more natural and biologically inspired. Among popular tissue engineering materials, poly(2-hydroxyethyl methacrylate) (pHEMA) has been widely investigated in conventional forms due to its biocompatibility, low toxicity, and hydrophilicity. However, the swelling of pHEMA in water remains a major concern. To address this issue, randomly oriented and aligned as-spun pHEMA nanofibrous scaffolds were first fabricated at speeds of 300 and 2000 rpm in this study, which were then post-treated using either a thermal or a freeze-drying method. In cell assays, human dermal fibroblasts (HDFs) adhered to the freeze-drying treated substrates at a significantly faster rate, whereas they had a higher cell growth rate on thermally-treated substrates. Results indicated that the structural properties of pHEMA nanofibrous scaffolds and subsequent cellular behaviors were largely dependent on post-treatment methods. Moreover, this study suggests that aligned pHEMA nanofibrous substrates tended to induce regular fibroblast orientation and unidirectionally oriented actin cytoskeletons over random pHEMA nanofibrous substrates. Such information has predictive power and provides insights into promising post-treatment methods for improving the properties of aligned pHEMA scaffolds for numerous tissue engineering applications.

Ya Li and Qian Shen contributed equally to this paper.

Supplementary Information The online version contains supplementary material available at https://doi.org/10.1007/s42765-020-00059-3.

✉ Jiadeng Zhu
zhujiadeng@gmail.com

1 College of Textile Science and Engineering (International Silk College), Zhejiang Sci-Tech University, 928 Second Avenue, Hangzhou 310018, China

2 National Engineering Laboratory for Modern Silk, College of Textile and Clothing Engineering, Soochow University, Suzhou 215123, Jiangsu, China

3 Putuo Hospital Affiliated to Shanghai University of Traditional Chinese Medicine, Shanghai 200062, China

4 Yancheng Hospital of Traditional Chinese Medicine Affiliated to Nanjing Universiy of Traditional Chinese Medicine, Yancheng 224000, Jiangsu, China

5 Chemical Sciences Division, Oak Ridge National Laboratory, Oak Ridge, TN 37831, USA

Graphic abstract

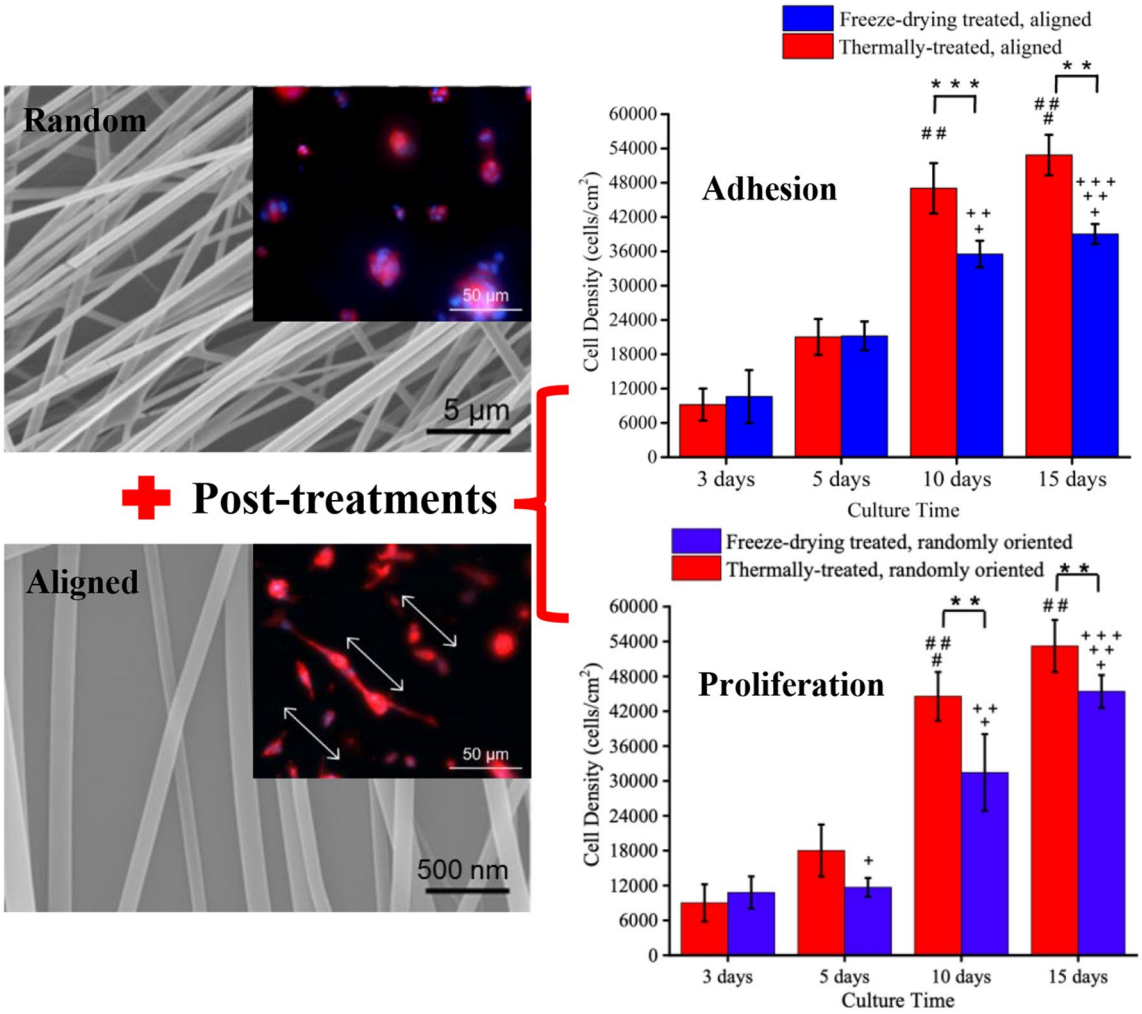

Keywords Electrospinning · Nanofibers · Aligned scaffolds · pHEMA · Post-treatment methods

Introduction

There are increasing numbers of tissue defects due to trauma which usually requires reconstructive procedures such as the blood vessel, skin, bone, and tendon repair in order to maintain normal tissue function [1–5]. The regeneration of injured or lost tissues needs that reparative cells assemble around and/or inside the supporting scaffold by a series of biological activities (e.g., adhesion, migration, proliferation, etc.) to achieve proper integration between cells and scaffolds, subsequently improving tissue regeneration [6–8].

In recent years, electrospinning technology, which has been widely performed as a fabrication method to generate nanofibers with diameters ranging from several nanometers to micrometers, has been developed to promote and repair damaged tissue function [9–11]. Also, nanofibers prepared by this novel approach can be axially aligned using an appropriate collecting mandrel. Previous studies indicated that aligned nanofiber structures could be obtained by a variety of collecting mandrel systems, including a rotating drum [12], parallel electrodes [13], and a rotating wire drum [14]. It has been demonstrated that electrospinning fabricates loosely connected 2D/3D porous scaffolds with high porosity and high surface area which can mimic extracellular matrix structures, making it as an excellent candidate for applications in tissue engineering [15–17].

In addition, a substantial number of human tissues and organs have parallel organized fiber structures such as the nervous, skeletal muscle, and ligament tissue [18–21]. It stands to reason that electrospun aligned nanofibrous scaffolds can apply in controlling the morphology of cells to be more natural and biologically-inspired [22]. Some previous

studies showed that parallel scaffolds could induce the morphology of cells into a biologically-inspired parallel structure [23, 24]. Therefore, to achieve parallel tissues for reconstruction, scaffolds with unidirectional orientation generated by electrospinning technology are critical. For example, Liu et al. reported that the process of HDF proliferation on the aligned poly(methyl methacrylate) (PMMA) fibers was more efficient than the sample of random PMMA fibers [25]. Also, Xu et al. suggested that aligned electrospun poly(l-lactid-*co*-ε-caprolactone) [P(LLA-CL)] nanofibrous scaffolds had the advantages of both synthetic biodegradable polymers and a stable architecture [26].

Among various candidates of polymer matrices, poly(2-hydroxyethyl methacrylate) (pHEMA) is a biodegradable polymer with good biocompatibility, hydrophilicity, and low toxicity, which lays a solid foundation for its potential application in the tissue scaffold field [27–29]. For instance, Ramalingam et al. demonstrated pHEMA nanofibrous scaffolds could have excellent biocompatibility for tissue engineering applications [30]. Rao et al. also illustrated the applicability of the prepared pHEMA and bamboo cellulose matrix composite fiber as a fibrous scaffold covering skin for treating skin cancer and wound healing [31]. Unfortunately, untreated pHEMA nanofibrous scaffolds appear noticeably swollen in water which is due to its hydrophilicity [32, 33]. In general, promoting internal cross-linking is performed to enhance hydrogel properties since water uptake can be controlled by cross-linking, which positions cross-linking as the main mechanism to optimize the water swelling. Rampichová et al. solved the problem of water instability of pHEMA microfibers by nebulization with phosphoric acid [34]. Mabilleau et al. added cross-linking agents to pHEMA and proved that the cross-linking method presented a significant decrease in swelling [35].

The objective of this study was to utilize aligned electrospun pHEMA nanofibrous scaffolds to induce the regeneration of fibroblasts. For this purpose, pHEMA nanofibrous scaffolds with different fiber orientations were first fabricated by electrospinning with adjusting rotation speeds from 300 to 2000 rpm. To solve the issue of water swelling caused by their hydrophilicity, electrospun scaffolds were post-treated using two different methods. One was to thermally treat the scaffolds which cross-linked pHEMA nanofibers and enhanced structural integrity. The other was to freeze-dry the scaffolds to accelerate de-swelling and enhance the ordered structure. Finally, fibroblasts were incubated on such scaffolds to investigate their adhesion, growth, and morphology.

In summary, the results demonstrated that the structural properties of electrospun pHEMA nanofibrous scaffolds and cell behaviors were found to significantly depend on subsequent treatment processes. The presently developed freeze-drying and thermal treatment methods were promising for improving the properties of pHEMA scaffolds for numerous tissue engineering applications. More importantly, this paper suggests that aligned pHEMA nanofibrous scaffolds could have a tendency to induce regular HDFs orientation and unidirectionally oriented actin cytoskeletons over randomly oriented pHEMA nanofibrous scaffolds.

Experimental

Electrospinning Set-Up

Certain amounts of pHEMA (Mw = 1,000,000, Sigma-Aldrich, Saint Louis, MO, USA) were added into *N*,*N*-dimethylformamide (DMF, Sigma-Aldrich) and the resultant polymer solutions were agitated by ultrasonic excitation to obtain uniformly mixed solutions followed by the electrospinning. A schematic illustration of the electrospinning setup was shown in Fig. S1. All the electrospinning experiments were carried out at constant temperature (25 °C) and humidity (40%). Briefly, the pHEMA/DMF blend solutions were electrospun using a high DC voltage power supply at a 25 kV potential between the solution and the collector with a receiving distance of 15 cm from the syringe tip. Solutions were delivered at a flow rate of 1.0 mL/h by a syringe pump. In order to study the effect of polymer concentrations, the pHEMA solutions were electrospun at different weight concentrations of 4, 8, 10, and 12 wt%. Moreover, both aligned and randomly oriented pHEMA nanofibers were fabricated by electrospinning under optimal conditions. Nanofibers were collected onto a rotating mandrel with rotation speeds at 300, 1000, 1500, and 2000 rpm, respectively.

Post-treatments

Electrospun scaffolds were post-treated by two different methods. One was to heat-treat the scaffold at 90 ºC for 48 h. The other was using freeze-drying, that was, the pHEMA scaffolds were frozen in a − 80 ºC freezer for 4 h and lyophilized in a LabconcoFreeZone® 2.5 Freeze Dry System (Kansas City, MO, USA) for 48 h at 60 Pa. Then, the organic solvent residues from pHEMA nanofibers were removed under vacuum for 48 h.

Morphology and Structure of Scaffolds

The morphology of pHEMA nanofibers and their sizes were examined by a scanning electron microscope (SEM, S-4800, Hitachi, Tokyo, Japan). The diameter and alignment of the nanofibers were determined by measuring one hundred nanofibers at different positions using NIH ImageJ 1.64 software (Shareware provided by the National Institutes of Health). The SEM images were opened in ImageJ and

measurements were calibrated using the scale bar on the images. For determining nanofiber orientation, a value of 0° denoted parallel alignment of the axis of the nanofiber and 90° represented perpendicular alignment.

X-ray diffraction (XRD, PANalytical Philips X-ray Diffractometer, X'Pert Pro, PANalytical, Almelo, Netherlands) was carried out to determine the crystalline content of the pHEMA powder with a 2θ range of 20°–60°. The functional groups of pHEMA nanofibers were analyzed by a Fourier transform-infrared spectroscopy (FT-IR, Thermo Nicolet Corporation, Nicolet 5700).

Contact Angle

The water contact angles of the untreated, thermally-treated, and freeze-drying treated scaffolds were measured via a Drop Shape Analyzer based contact angle measuring device (DSA Registered Version) as per the instruction manual.

Swelling Measurements

Considering the hydrophilicity of electrospun pHEMA nanofibers, the swelling measurements were conducted at constant temperature (25 °C) and humidity (40%). The electrospun pHEMA nanofibrous scaffolds were soaked in a solvent of phosphate buffer saline (PBS, Sigma-Aldrich). The swelling behavior of pHEMA nanofibrous scaffolds was also tested at room temperature for a period of 72 h. At selected time points (0, 2, 4, 6, 12, 18, 30, 42, 66 and 72 h) the nanofibrous scaffolds were taken out and weighed after removal of excess surface water with a Kimwipe (Sigma-Aldrich). The swelling weight increase of pHEMA nanofibrous scaffolds was calculated according to the following equation:

$$\text{Swelling weight increase ratio (\%)} = \left(W_{wet} - W_{dry}\right) / W_{dry} \times 100\% \quad (1)$$

where W_{wet} was the weight of the scaffold after removal of water and W_{dry} was the weight of the initial scaffold.

Cell Culture

HDFs, purchased from the American Type Culture Collection (ATCC, Manassas, VA, USA; catalog number PCS-201-012™, population numbers 6–8), were cultured in Dulbecco's Modified Eagle Medium (DMEM, Sigma-Aldrich) with 10 wt% fetal bovine serum (FBS, Sigma-Aldrich) and 1 wt% penicillin/streptomycin (P/S, HyClone; Thermo Fisher Scientific, Waltham, MA, USA) by weight in a 37 °C, humidified, 5% CO_2/95% air environment.

Cell Adhesion

Electrospun pHEMA nanofibrous scaffolds were placed individually into the wells of a 96-well plate (Fig. S2a) and sterilized under UV light for 0.5 h each side. Before cell seeding, samples were preconditioned with serum-free DMEM for 2 h to improve cell adhesion. HDFs were then seeded onto scaffolds at a density of approximately 10,000 cells/cm^2 and incubated under standard culture conditions (Fig. S2b). Cell adhesion was measured after 2, 4, 6, 8 and 10 h of incubation. At each time point, samples were rinsed with PBS and fresh media DMEM 100 µL was added to each well along with an MTS (Promega Corporation, Fitchburg, WI, USA) dye in a 5:1 ratio by weight (media: MTS). Samples were incubated for 4 h to allow the MTS dye to completely react with the metabolic products of the adherent HDFs. The absorbance of an MTS solution was measured at a wavelength of 490 nm using a SpectraMax M3 (Molecular Devices, Sunnyvale, CA, USA) microplate reader. The number of adherent cells was determined by comparing the resulting absorbance values to a standard curve constructed at the beginning of each trial. Experiments were run in triplicate (n = 3) and repeated three times (N = 3).

Cell Proliferation

An aliquot of 5,000 cells/cm^2 was seeded onto the surface of a pre-wetted electrospun pHEMA nanofibrous scaffold placed in 96-well culture plates. Cell proliferation was tested with an MTS dye after 3, 5, 10, and 15 days. During the period, the media was changed every day by replacing half of the original volume with an equal volume of fresh media. The process used to determine cell proliferation was the same as that used to determine cell adhesion.

Cell Morphology

HDFs were seeded on the sterilized, randomly oriented and aligned electrospun pHEMA nanofibrous scaffolds placed in 24-well culture plates at a concentration of 10,000 cells/cm^2 and were cultured for 3 days.

After the 3-day incubation, samples were fixed with a 4 wt% paraformaldehyde solution diluted in PBS for 1 h at 4 ºC. After permeabilization with a 0.1 wt% Triton-X/0.1 wt% Tween solution (Sigma-Aldrich) for 10 min and blocking in PBS containing 1 wt% bovine serum albumin for 1 h at room temperature, HDFs were incubated with 5 wt% BSA in PBS overnight at 4 ºC. The following day, HDFs were incubated with diluted FITC-anti-vinculin 1:800 in 1 wt% BSA in PBS and added to cells for 20 min at room temperature, preventing light exposure. Subsequently, diluted Alexa Fluor 568 Phalloidin 1:25 in 1 wt% BSA in PBS and added to the cells for 20 min. Finally, samples were visualized with inverted

Confocal Laser Scanning Microscopy system (CLSM 700; Carl Zeiss Meditec AG, Jena, Germany). All the percentages were based on mass fraction.

Statistical Analysis

For all cell culture assays, the reported arithmetic means and standard deviation refer to the average of three independent experiments, using three replicates per each group. Statistical comparisons between groups were performed with a two-tailed Student's t test and differences were considered significant if $p < 0.05$.

Results and Discussion

Figure 1 shows the surface morphology of the electrospun nanofibrous scaffolds. It was found that nanofiber formation was strongly dependent on the concentration of pHEMA. When the weight concentration of pHEMA in the pHEMA/DMF solution was 4%, nanofibers were not able to be formed (Fig. 1a). With increasing concentrations, the percent of droplet decreased, while the percent of nanofiber increased, as shown in Fig. 1b, c. When the concentration of pHEMA/DMF achieved to 12 wt%, the number of nanofibers further increased and exhibited a homogeneous morphology which can be seen in Fig. 1d. However, it was difficult to fully dissolve the pHEMA polymer to form a homogeneous and transparent solution while further increasing the concentration. Thus, a 12 wt% solution concentration would be the optimal fabrication condition.

Electrospun pHEMA nanofibrous scaffolds with different fiber angles were generated at various rotation rates of 300, 1000, 1500, and 2000 rpm. A progressive increase in fiber orientation was observed as the rotation rate increased (Fig. 2a–h). It was anticipated that the highly oriented nanofibrous scaffolds were produced when rotation speed was increased to 2000 rpm, whereas the randomly oriented nanofibrous scaffolds were fabricated at 300 rpm, and these conditions were chosen as the counterparts in the following cell culture studies.

For the aligned nanofibers generated at the rotation rate of 2000 rpm, as shown in Fig. S3a, the average diameter was about 80.2 nm with the majority of fiber diameters ranged from 40 to 100 nm. However, for the random nanofibers shown in Fig. S3b, the majority of fiber diameters ranged from 60 to 120 nm with an average diameter of 106.4 nm. It was noticed that all the smallest, average, and largest diameter of aligned fibers were smaller than those of the random fibers obtained from the same processing conditions. Fiber orientation was increased significantly as the rotation speed increased. This is probably because of the increased tensile properties with rotational deposition [20]. Thus, the highly oriented and random nanofibrous scaffolds were prepared at 2000 and 300 rpm, respectively.

The results indicated that the fiber diameters were directly related to the rotation rates. One reason behind the change of diameters may be explained by considering the high rotation speeds of the rotating mandrel, which exerted a

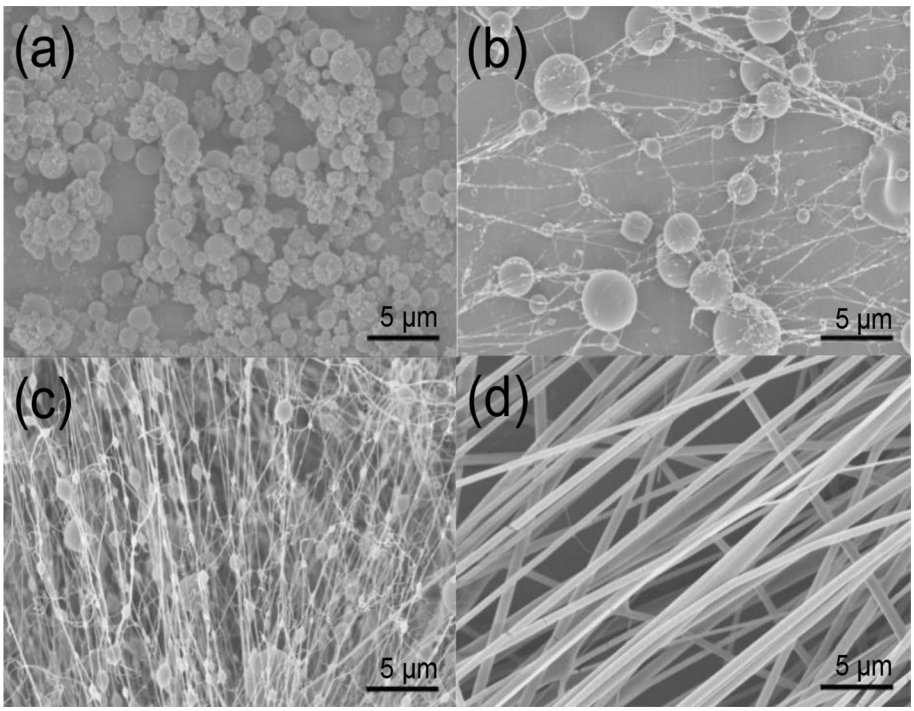

Fig. 1 SEM images of electrospun pHEMA nanofibers at various polymer solution concentrations: **a** 4 wt%, **b** 8 wt%, **c** 10 wt%, and **d** 12 wt%

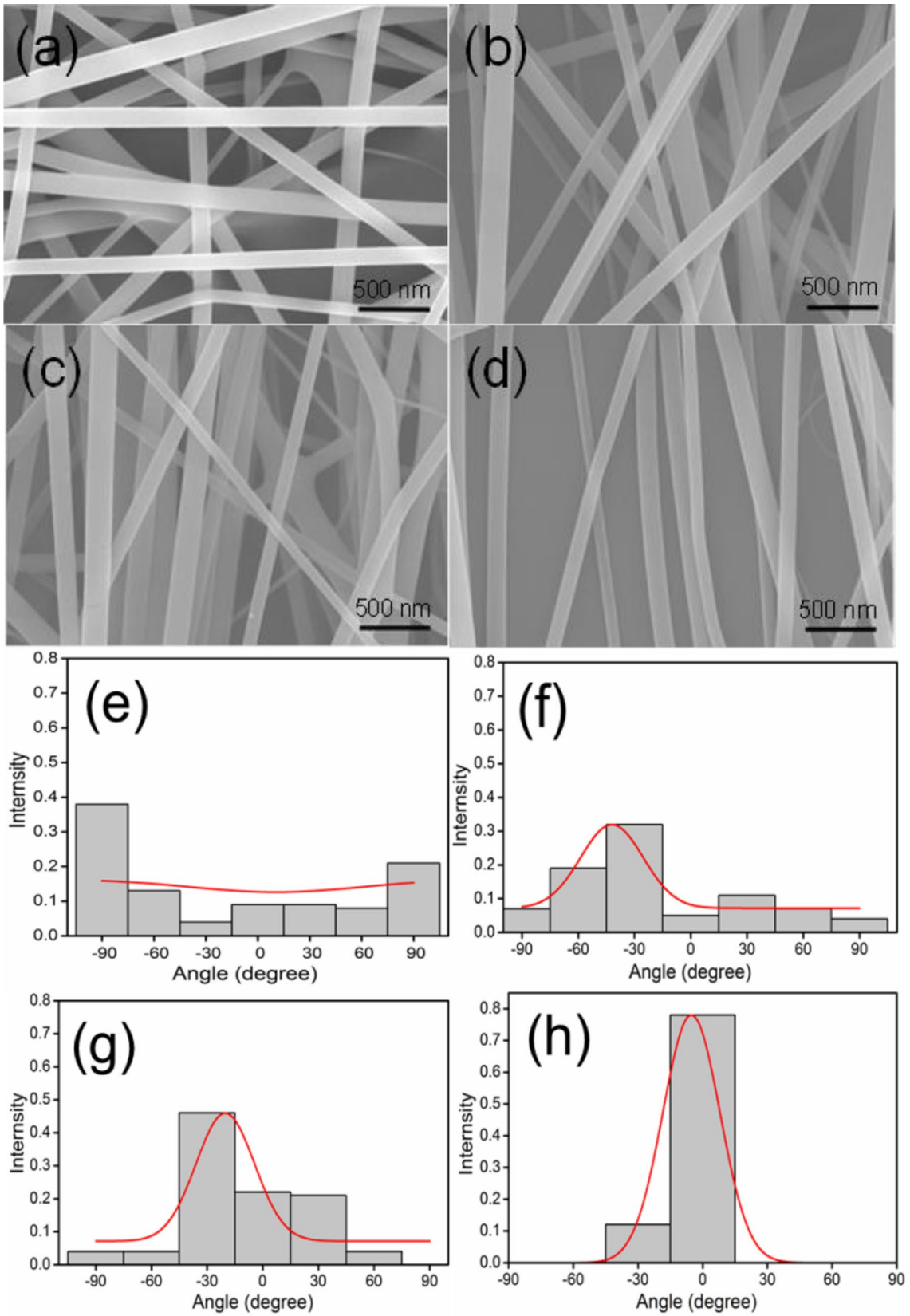

Fig. 2 Nanofiber angles for the different rates of rotation: **a**–**d** SEM images of pHEMA nanofibers and **e**–**h** histograms of fiber angle, **a**, **e** 300 rpm, **b**, **f** 1000 rpm, **c**, **g** 1500 rpm, and **d**, **h** 2000 rpm

tangential force on the syringe tip to stretch the resulting fibers [36]. Although a small difference in fiber diameters existed between the aligned and random nanofibrous scaffolds, diameters of the aligned and random electrospun fiber were in the same nanoscale regime. Therefore, it suggests that fiber diameter would not play a prominent role on the different behavior of cells as will be described. Just as Yim et al. demonstrated, the alignment of smooth muscle cells differed only when the half pitch of the nanogratings was varied from 350 nm to 2 μm, which meant no significant difference existed under the same scale [37].

Even though considerable research to develop pHEMA based materials for tissue engineering applications have been done [27–29], the swelling of pHEMA in aqueous solution is still a huge challenge [32]. In this study, we post-treated the electrospun pHEMA scaffolds using either a thermal treatment or a freeze-drying method. When untreated pHEMA nanofibrous scaffolds (Fig. S4a) were soaked in water, nanofibers appeared noticeably swollen within a short time (Fig. S4b). Figure 3a–i shows the morphology of untreated, thermally treated and freeze-drying treated scaffolds after being soaked in water for different times. Fig. S4b and Fig. 3d, g display that the surface morphology of the untreated scaffolds appeared severely swollen after soaking in water, causing the surface fibers to merge. For the thermally treated scaffolds, the morphology of the samples remained unchanged until 48 h or even 72 h, which indicated that the rate of swelling in water was significantly reduced (Fig. 3b, e, h). However, for the freeze-drying treated scaffolds (Fig. 3c, f, i), the swelling process mainly occurred after 24 h. In summary, during the first 24 h, a freeze-drying treatment method had a better effect on reducing the swelling rate, while with an increase of time, the advantage of a 90 ℃ thermal-treatment method further became apparent.

Both approaches above helped preserve nanofiber structure, and thus are a key step in the formation of stable electrospun pHEMA scaffolds. It was clearly seen from Fig. 4a that untreated pHEMA was highly hydrophilic

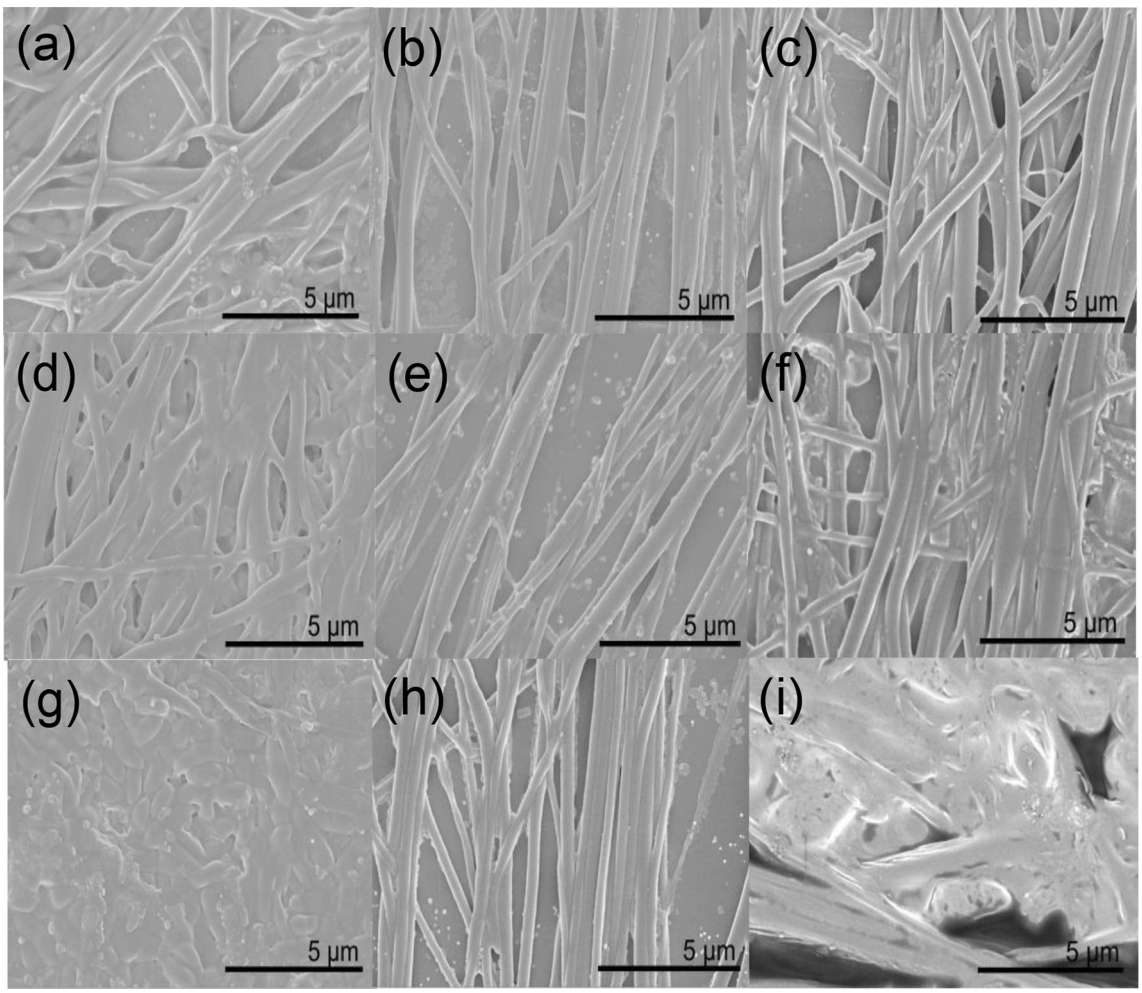

Fig. 3 SEM images of nanofibers after 24 h (**a**–**c**), 48 h (**d**–**f**), and 72 h (**g**–**i**) of water incubation for untreated (**a**, **d**, **g**), thermally-treated (**b**, **e**, **h**), and freeze-drying treated (**c**, **f**, **i**) scaffolds

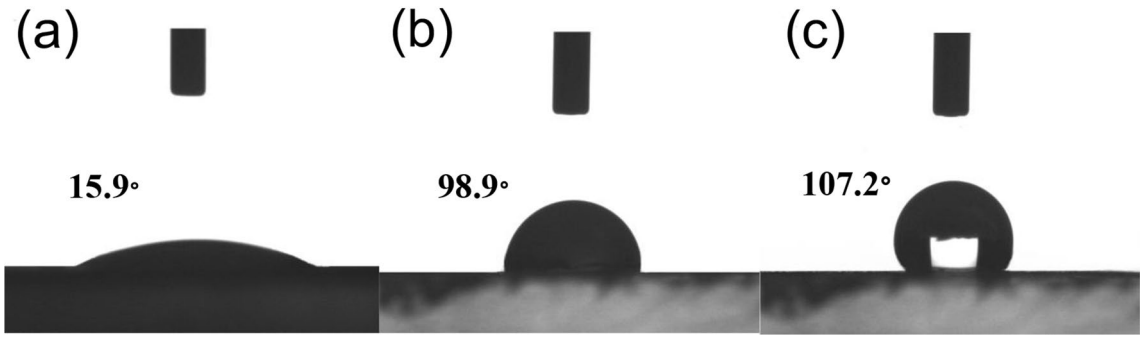

Fig. 4 Water-contact angles of **a** untreated, **b** thermally treated and **c** freeze-drying treated scaffolds

(water-contact angle value of 15.9°). However, the high water-contact angle values obtained for thermally treated (Fig. 4b) and freeze-drying (Fig. 4c) scaffolds (98.9° and 107.2°, respectively), indicated that the post-treated scaffolds were hydrophobic. Water contact angle studies also demonstrated that both the thermal and freeze-drying treatment methods are strategies for modulating the nanofiber performance.

In order to understand the mechanism of reducing water swelling using the thermal and freeze-drying treatment methods, we conducted analyses of the swelling weight increase ratio as exhibited in Fig. 5a. For untreated scaffolds, the weight increase ratio mainly occurred during the first 18 h up to 24.9%, while the swelling weight began to decrease after that. After the freeze-drying treatment, the change of swelling weight had the similar trend as untreated samples, but it had lower swelling weight increase and the weight increase was significantly reduced after 18 h, which might because the nanofiber scaffolds had degenerated in water after that point. However, the thermally treated scaffolds approximately remained unchanged for the first 18 h and slightly increased afterwards, which meant that the thermally treated scaffolds had the lowest swelling rate compared to the untreated and freeze-drying treated scaffolds.

To further investigate the possible structural change of electrospun pHEMA nanofibers caused by different post-treatment methods, the XRD spectra of the electrospun pHEMA fibers before and after post-treatments were presented in Fig. 5b. A broad peak at $2\theta = 21.2°$ was recorded for the untreated scaffold [38]. However, with the thermal post-treatment, the broad peak slightly shifted to 18.4°. In contrast, the characteristic X-ray peak evolved to 22.4° for the freeze-dried one. Besides, Fig. S5a and b provided the FT-IR results for the three kinds of pHEMA nanofibers. It was seen that, due to the post-treatment methods, the peak at about 1604 cm^{-1} for untreated scaffold, corresponding to $v_{C–C}$, appeared to have some position shifts. Therefore, the absorptivity ratios of $v_{C–C}$ to $v_{C–O}$ were 0.537, 0.098 and 0.262 for untreated, thermally treated and freeze-drying treated pHEMA nanofibers, respectively. These results suggested that the absorptivity ratio of pHEMA nanofibers would be reduced after the thermal and freeze-drying

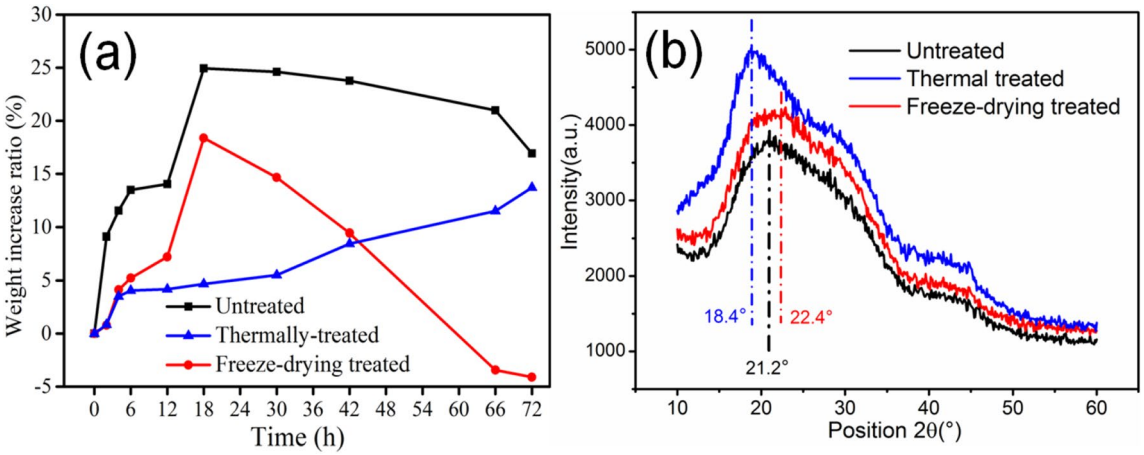

Fig. 5 **a** Studies of swelling weight increase ratios after different treatments. **b** XRD patterns of untreated, thermally treated and freeze-drying treated pHEMA nanofibers

treatment methods. The X-ray and FTIR peaks shown some shifts which might be attributed to the interaction between the hydroxyl groups [31]. During the thermal treatment process, the unreacted monomers were further polymerized, which led to increased scaffold integrity [32]. Likely, during the freeze-drying process, hydrogel pHEMA scaffolds shrunk, resulting in a slight bending of the composite [39, 40].

XRD and FTIR performed on the thermally and freeze-drying treated scaffolds revealed that the free radical polymerization was incomplete in untreated scaffolds and progressed further during the thermal and freeze-drying treatment processes. Thus, the slightly changed internal structure shown in the XRD and FTIR spectra might play an important role in optimizing the rate of weight absorption, potentially leading to improved stability of electrospun pHEMA nanofibrous scaffolds.

Figure S6 illustrated the relationship between the absorbance value and cell number by curve-fitting, which could be obtained as

$$y = -8273 + 39872x \quad (2)$$

When the absorbance value became bigger, more cells were produced, HDFs adhesion and proliferation would be better.

Figure 6a shows that HDFs adhered to both thermally and freeze-drying treated pHEMA substrates. In particular, statistical analysis using ANOVA also provided evidence that HDFs adhered to the freeze-drying treated nanofibrous substrate at a significantly faster rate than the thermally treated nanofibrous substrate at 2 and 4 h. Furthermore, while compared with the number of HDFs at 2 h, much more cells were found attached to the freeze-drying treated substrate compared to the other substrates at 6 h. The number of HDFs that adhered to the thermally treated substrate caught up with the number of adherent cells on the freeze-drying treated substrate until 8 h. By 10 h, the percentages of HDFs that adhered to the thermal and freeze-drying treated substrates were 73.22 and 79.54%, respectively.

The mechanism of the observation was possible that the freeze-drying treatment method had a better effect on maintaining the morphology of nanofibers by reducing the swelling rate at the first 24 h. In addition, the proposed mechanism illustrated that excellent nanofiber structure could induce, enhance, and guide cell adhesion [41]. Due to the increased rates of cell adhesion, cells were allowed to adhere into the wound or damaged tissues within a shorter time period, which could expend applications of nanofiber substrates.

HDFs proliferation tests conducted after 3, 5, 10, and 15 days (Fig. 6b, c) indicated increasing numbers of HDFs on the four substrates (thermally treated oriented and random pHEMA scaffolds, freeze-drying treated oriented and random pHEMA scaffolds) during the culture period. Especially, on day 10 and 15, much more cells attached on the four substrates compared with day 3 and 5. Moreover, Fig. 6b, c revealed that the densities of HDFs were similar for all substrates after 3 and 5-day incubation. Nevertheless, differences in the cell density became significant on day 10 and 15, where cell densities on the thermally treated substrates were dramatically higher than the freeze-drying treated substrates for both aligned and randomly oriented substrates. Because of the increased rate of cell growth, cells might be able to adhere into a wound or damaged tissue after the application of thermally treated pHEMA (as compared to freeze-drying treated) under a shorter time frame allowing for quicker growth and tissue formation.

Because HDFs had a higher cell growth rate on the thermally treated pHEMA nanofibrous substrates, the results of cell proliferation contradicted the cell adhesion studies' results. This could be explained since the freeze-drying treated substrates had a clearer nanofiber morphology during the first 24 h, whereas after day 3, 5, 10, and 15, advantages of the thermally treated substrates towards reducing pHEMA swelling increased. Another possible explanation might be that different seeding densities were used in the adhesion and proliferation assays with the latter using half of the number of cells for experimental ease. The adhesion assays demonstrated that at 8 and 10 h, no obvious differences existed between the two substrates, likely since the cell density was approximately two-times higher than the initial seeding density [42]. Therefore, it was reasonable that the advantages of thermally treated substrates increased over freeze-drying treated substrates in the cell proliferation assay.

Besides, statistical analysis combined with Fig. 6b, c depicted that cell densities in the cell proliferation assay were similar between the random and aligned electrospun pHEMA substrates for both scaffolds treated by the thermal and freeze-drying methods. The results indicated that the HDF proliferation rate seemed to be independent of the fiber alignment, but related to post-treatment methods, suggesting that the thermal treatment method strongly supported and/or improved HDFs growth as compared to the freeze-drying treatment method.

Since the thermal treatment method had an average 25% increase in the number of cells based on the results mentioned above, we used the thermally treated aligned and randomly oriented scaffolds to determine whether the alignment of fibers affected cell morphology. Figure 7a displays that HDFs were randomly organized along the randomly oriented nanofibrous substrate and they were distributed into islands and separated from one another. Conversely, the cells on the aligned substrate tended to grow along the fibers after cell seeding (Fig. 7b). In addition, on the random substrate, the

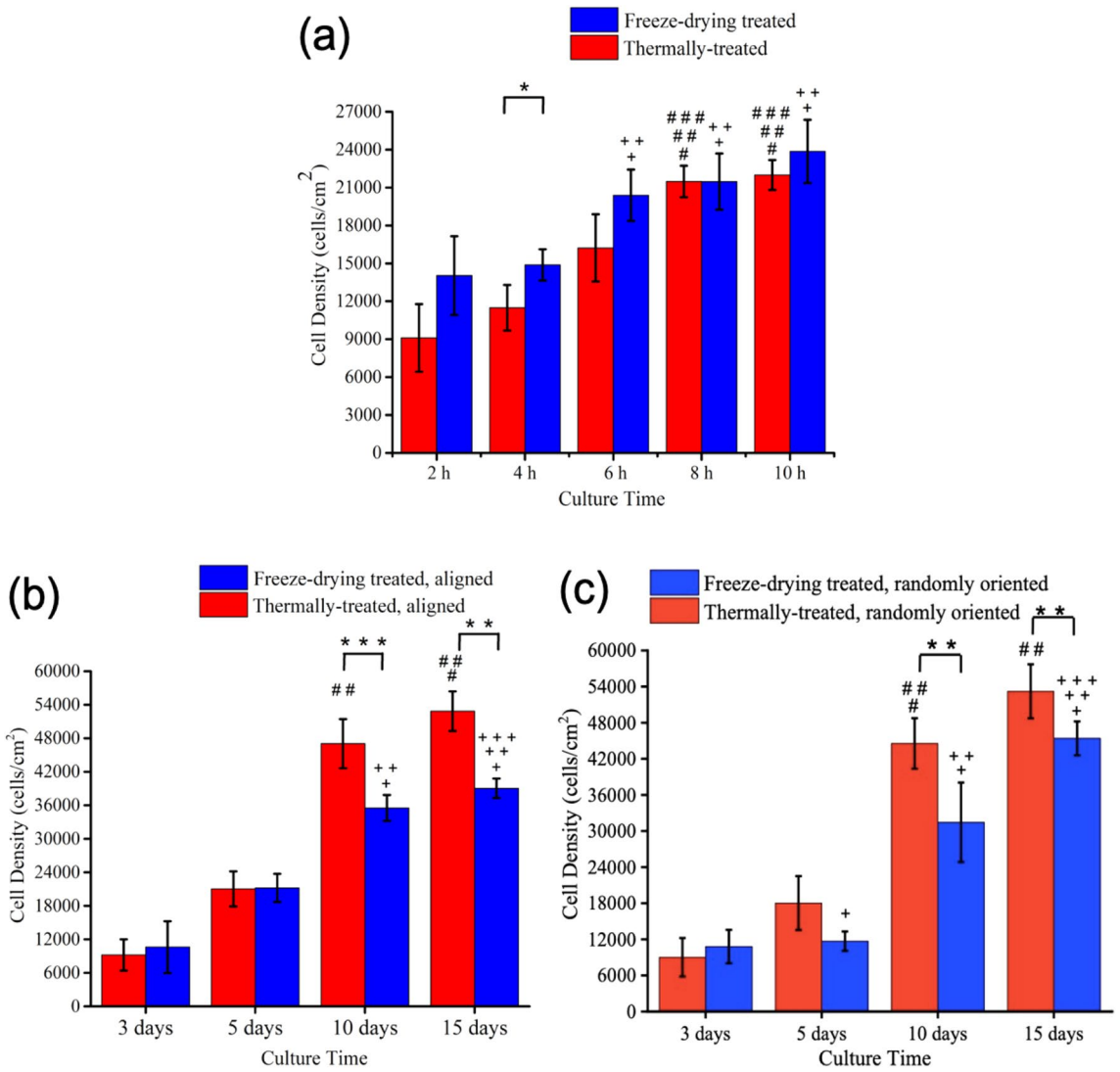

Fig. 6 **a** Adhesion density of HDFs to the electrospun nanofibrous substrates after various culture times. Date = mean ± St. Dev; N = 3, $^{*}p < 0.05$; $^{\#}p < 0.05$ compared with 2 h adhesion on the thermally-treated substrates; $^{\#\#}p < 0.05$ compared with 4 h adhesion on the thermally-treated substrates; $^{\#\#\#}p < 0.05$ compared with 6 h adhesion on the thermally-treated substrates; $^{+}p < 0.05$ compared with 2 h adhesion on the freeze-drying treated substrates; $^{++}p < 0.05$ compared with 4 h adhesion on the freeze-drying treated substrates. **b**, **c** Density of HDFs after 3, 5, 10, and 15 days of culture on aligned and random substrates, respectively. Date = mean ± St. Dev; N = 3, $^{**}p < 0.01$, $^{***}p < 0.001$; $^{\#}p < 0.05$ compared with day 3 proliferation on the thermally-treated aligned and the random substrates, respectively; $^{\#\#}p < 0.05$ compared with day 5 proliferation on the thermally-treated aligned and random substrates, respectively; $^{+}p < 0.05$ compared with day 3 proliferation on the freeze-drying treated aligned and random substrates, respectively; $^{++}p < 0.05$ compared with day 5 proliferation on the freeze-drying treated aligned and random substrates, respectively; and $^{+++}p < 0.05$ compared with day 10 proliferation on the freeze-drying treated aligned and random substrates, respectively

cell actin cytoskeleton was mostly scattered in all directions (Fig. 7c), while the cell actin cytoskeleton aligned with the direction of the nanofibers for the oriented one (Fig. 7d). Moreover, when cells and the cell actin cytoskeleton were disparate between the aligned and randomly oriented substrates, we could see that the aligned structures had tremendous potential for even greater growth. Hence, significant differences in cell morphology based on fiber morphology could contribute to aligned nanofiber structures like natural extracellular structures inducing more biologically inspired focal contacts and other cell attachment structures [43].

Conclusions

This study explored the influence of electrospun pHEMA nanofibrous scaffolds on the function of fibroblasts. The results showed that the morphology of electrospun pHEMA

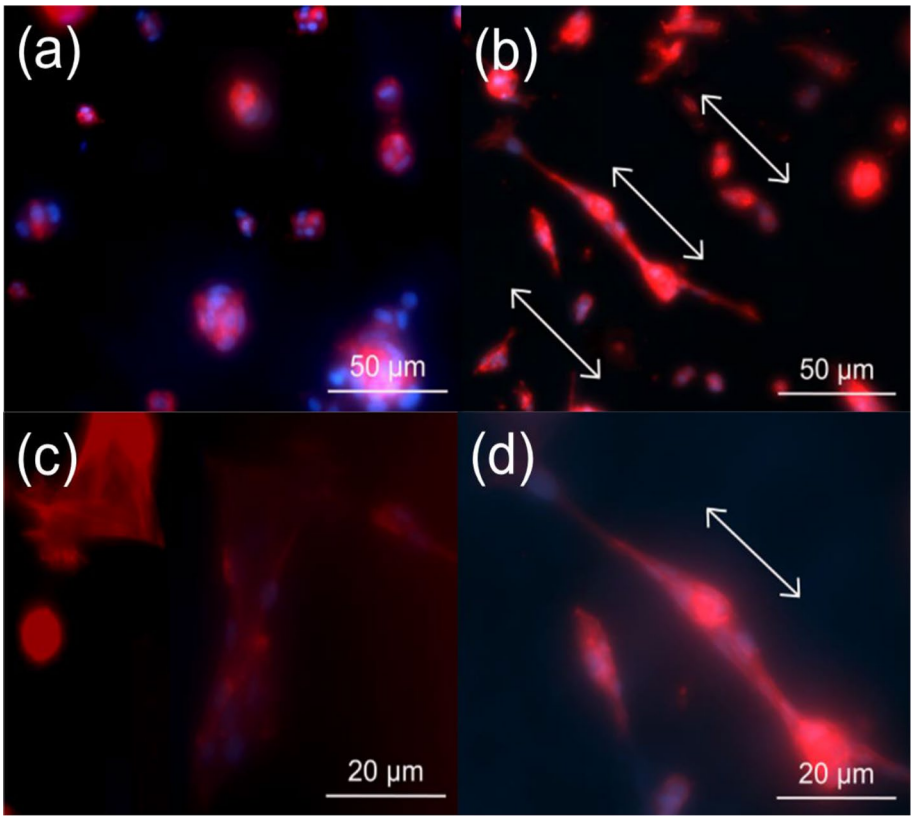

Fig. 7 Fluorescence images of HDFs seeded for 3 days on electrospun substrates with different orientations. **a**, **c** Randomly oriented and **b**, **d** aligned substrates

was strongly affected by the concentration of the polymeric solution, and a 12 wt% pHEMA solution concentration was the optimal fabrication condition. The randomly oriented and aligned nanofibrous scaffolds were fabricated when rotation speeds were 300 and 2000 rpm, respectively. Additionally, analyses of swelling weight, contact angle, and XRD spectra demonstrated that the swelling in an aqueous solution was improved remarkably after the freeze-drying or thermal treatment method. The freeze-drying treated scaffolds had lower swelling after the first 24 h, whereas advantages of the thermal treatment method increased after 24 h. Moreover, the freeze-drying treated scaffolds induced the adhesion of HDFs at a significantly faster rate than that of the thermally treated scaffolds especially after 4 h. However, HDFs proliferated with a significant higher cell growth rate on the thermally treated pHEMA nanofibrous scaffolds than the freeze-drying treated scaffolds after 10 and 15 days of incubation. Ultimately, for electrospun aligned substrates, cells and the cell actin cytoskeleton were observed to align and elongate along the fiber axes which suggested that a unidirectional fiber orientation can guide HDFs and cell actin cytoskeleton alignment. In summary, this study recommends the fabrication of an electrospun aligned pHEMA nanofibrous scaffold followed by freeze-drying or thermal as a promising method for enhancing fibroblast adhesion and growth, which can be investigated for a wide range of tissue engineering applications.

Acknowledgements The authors appreciate Northeastern University for funding. The work is also supported by Priority Academic Program Development of Jiangsu Higher Education Institutions (PAPD), National Natural Science Foundation of China (Grant no. 11372205 and 31900964), Program of Zhejiang Sci-Tech University (Grant no. 11110231281803), Scientific Research Foundation of Zhejiang Sci-Tech University (Grant no. 11112932618215) and the Fundamental Research Funds of Zhejiang Sci-Tech University (Grant no. 2020Q002).

Compliance with ethical standards

Conflict of interest On behalf of all authors, the corresponding author states that there is no conflict of interest.

References

1. Punnakitikashem D, Truong JU, Menon KT, Nguyen YH. Electrospun biodegradable elastic polyurethane scaffolds with dipyridamole release for small diameter vascular grafts. *Acta Biomater*. **2014**;*10*(11):4618–28.
2. Jin G, Prabhakaran MP, Ramakrishna S. Stem cell differentiation to epidermal lineages on electrospun nanofibrous substrates for skin tissue engineering. *Acta Biomater*. **2011**;*7*(8):3113–22.
3. Norouzi M, Boroujeni SM, Omidvarkordshouli N, Soleimani M. Advances in skin regeneration: application of electrospun scaffolds. *Adv Healthc Mater*. **2015**;*4*(8):1114–33.
4. Yin Z, Chen X, Chen JL, Shen WL, Hieu Nguyen TM, Gao L, Ouyang HW. The regulation of tendon stem cell differentiation by the alignment of nanofibers. *Biomaterials*. **2009**;*31*(8):2163–7215.

5. De MA, Seifalian AM, Birchall MA. Orchestrating cell/material interactions for tissue engineering of surgical implants. *Macromol Biosci*. **2012**;*12*(8):1010–21.
6. Cordie T, Harkness T, Jing X, Carlson-Stevermer J, Mi HY, Turng LS. Nanofibrous electrospun polymers for reprogramming human cells. *Cell Mol Bioeng*. **2014**;*7*(3):379–93.
7. Morgado PI, Aguiar-Ricardo A, Correia IJ. Asymmetric membranes as ideal wound dressings: an overview on production methods, structure, properties and performance relationship. *J Membr Sci*. **2015**;*490*:139–51.
8. Sheikh FA, Ju HW, Lee JM, Bo MM, Park HJ, Lee OJ. 3D electrospun silk fibroin nanofibers for fabrication of artificial skin. *Nanomed Nanotechnol*. **2015**;*11*(3):681–91.
9. Baker BM, Mauck RL. The effect of nanofiber alignment on the maturation of engineered meniscus constructs. *Biomaterials*. **2007**;*28*(11):1967–77.
10. Talebian S, Foroughi J, Wade SJ, Vine KL, Dolatshahi-Pirouz A, Mehrali M, Conde J, Wallace GG. Biopolymers for antitumor implantable drug delivery systems: recent advances and future outlook. *Adv Mater*. **2018**;*30*(31):1706665.
11. Chen SH, Chang Y, Lee KR, Lai JY. A three-dimensional dual-layer nano/microfibrous structure of electrospun chitosan/poly(d,l-lactide) membrane for the improvement of cytocompatibility. *J Membr Sci*. **2014**;*450*:224–34.
12. Choi JS, Lee SJ, Christ GJ, Atala A, Yoo JJ. The influence of electrospun aligned poly(epsilon-caprolactone)/collagen nanofiber meshes on the formation of self-aligned skeletal muscle myotubes. *Biomaterials*. **2008**;*29*(19):2899–906.
13. Hutchins-Kumar LD, Wang J, Tuzhi P. Parallel dual-electrode detection based on size exclusion for liquid chromatography/electrochemistry. *Anal Chem*. **1986**;*58*(6):1019–23.
14. Katta P, Alessandro M, Ramsier RD, Chase GG. Continuous electrospinning of aligned polymer nanofibers onto a wire drum collector. *Nano Lett*. **2004**;*4*(11):2215–8.
15. Liu SJ, Kau YC, Chou CY, Chen JK, Wu RC, Yeh WL. Electrospun plga/collagen nanofibrous membrane as early-stage wound dressing. *J Membr Sci*. **2010**;*355*:53–9.
16. Agarwal S, Wendorff JH, Greiner A. Use of electrospinning technique for biomedical applications. *Polymer*. **2008**;*49*(26):5603–21.
17. Yang C, Deng G, Chen W, Ye XJ, Mo XM. A novel electrospun-aligned nanoyarn-reinforced nanofibrous scaffold for tendon tissue engineering. *Colloid Surf B*. **2014**;*122*:270–6.
18. Hurme T, Kalimo H, Lehto M, Jarvinen M. Healing of skeletal muscle injury: an ultrastructural and immunohistochemical study. *Med Sci Sport Exerc*. **1991**;*23*(7):801–10.
19. Chew SY, Mi R, Hoke A, Leong KW. Aligned protein-polymer composite fibers enhance nerve regeneration: a potential tissue engineering platform. *Adv Funct Mater*. **2007**;*17*(8):1288–96.
20. Lee CH, Shin HJ, Cho IH, Kang YM, Kim IM, Park KD. Nanofiber alignment and direction of mechanical strain affect the ECM production of human ACL fibroblast. *Biomaterials*. **2005**;*26*(11):1261–70.
21. Qin S, Clark RA, Rafailovich MH. Establishing correlations in the en-mass migration of dermal fibroblasts on oriented fibrillar scaffolds. *Acta Biomater*. **2015**;*25*:230–9.
22. Kai D, Prabhakaran MP, Jin G, Ramakrishna S. Guided orientation of cardiomyocytes on electrospun aligned nanofibers for cardiac tissue engineering. *J Biomed Mater Res B*. **2011**;*98*(2):379–86.
23. Chew SY, Mi R, Hoke A, Leong KW. The effect of the alignment of electrospun fibrous scaffolds on Schwann cell maturation. *Biomaterials*. **2008**;*29*(6):653–61.
24. Mi HY, Salick MR, Jing X, Crone WC, Peng XF, Turng LS. Electrospinning of unidirectionally and orthogonally aligned thermoplastic polyurethane nanofibers: fiber orientation and cell migration. *J Biomed Mater Res A*. **2015**;*103*(2):593–603.
25. Liu Y, Ji Y, Ghosh K, Clark RAF, Huang L, Rafailovich MH. Effects of fiber orientation and diameter on the behavior of human dermal fibroblasts on electrospun PMMA scaffolds. *J Biomed Mater Res A*. **2009**;*90*(4):1092–106.
26. Xu CY, Inai R, Kotaki M, Ramakrishna S. Aligned biodegradable nanofiber structure: a potential scaffold for blood vessel engineering. *Biomaterials*. **2004**;*25*(5):877–86.
27. Dragusin DM, Van Vlierberghe S, Dubruel P, Dierick M, Van Hoorebeke L, Declercq HA, Cornelissen MM, Stancu IC. Novel gelatin-PHEMA porous scaffolds for tissue engineering applications. *Soft Matter*. **2012**;*8*(37):9589–602.
28. Atzet S, Curtin S, Trinh P, Bryant S, Ratner B. Degradable poly(2-hydroxyethyl methacrylate)-*co*-polycaprolactone hydrogels for tissue engineering scaffolds. *Biomacromol*. **2008**;*9*(12):3370–7.
29. Badea A, Mccracken JM, Tillmaand EG, Kandel ME, Oraham AW, Mevis MB, Rubakhin SS, Popescu G, Sweedler JV, Nuzzo RG. 3D-printed pHEMA materials for topographical and biochemical modulation of dorsal root ganglion cell response. *ACS Appl Mater Interfaces*. **2017**;*9*(36):30318–28.
30. Ramalingam N, Natarajan TS, Rajiv S. Development and characterization of electrospun poly(2-hydroxy ethyl methacrylate) for tissue engineering applications. *Adv Polym Tech.* **2013**;*32*(3):617–29.
31. Rao SS, Jeyapal SG, Rajiv S. Biodegradable electrospun nanocomposite fibers based on poly(2-hydroxy ethyl methacrylate) and bamboo cellulose. *Compos Part B Eng*. **2014**;*60*:43–8.
32. Zhang B, Lalani R, Cheng F, Liu Q, Liu L. Dual-functional electrospun poly(2-hydroxyethyl methacrylate). *J Biomed Mater Res A*. **2011**;*99*(3):455–66.
33. Hennink WE, De Jong SJ, Bos GW, Veldhuis TFJ, Van Nostrum CF. Biodegradable dextran hydrogels crosslinked by stereocomplex formation for the controlled release of pharmaceutical proteins. *Int J Pharm*. **2004**;*277*(1–2):99–104.
34. Rampichová M, Martinová L, Košťáková E, Filová E, Míčková A, Buzgo M, Buzgo M, Michálek J, Přádný M, Nečas A, Lukáš D, Amler E. A simple drug anchoring microfiber scaffold for chondrocyte seeding and proliferation. *J Mater Sci Mater Med*. **2012**;*23*(2):555–63.
35. Mabilleau G, Stancu IC, Honoré T, Legeay G, Cincu C, Baslé MF, Chappard D. Effects of the length of crosslink chain on poly(2-hydroxyethyl methacrylate) (pHEMA) swelling and biomechanical properties. *J Biomed Mater Res A*. **2006**;*77*(1):35–42.
36. Yang F, Murugan R, Wang S, Ramakrishna S. Electrospinning of nano/micro scale poly(l-lactic acid) aligned fibers and their potential in neural tissue engineering. *Biomaterials*. **2005**;*26*(15):2603–10.
37. Hu W, Yim EKF, Reano RM, Leong KW, Pang SW. Effects of nanoim printed patterns in tissue-culture polystyrene on cell behavior. *J Vac Sci Technol B*. **2005**;*23*(6):2984–9.
38. Ramalingam N, Natarajan TS, Rajiv S. Preparation and characterization of electrospun curcumin loaded poly(2-hydroxyethyl methacrylate) nanofiber-A biomaterial for multidrug resistant organisms. *J Biomed Mater Res A*. **2015**;*103*(1):16–24.
39. Song J, Saiz E, Bertozzi CR. Preparation of pHEMA-CP composites with high interfacial adhesion via template-driven mineralization. *J Eur Ceram Soc*. **2003**;*23*(15):2905–19.
40. Song K, Zhu W, Li X, Yu Z. A novel mechanical robust, self-healing and shape memory hydrogel based on PVA reinforced by cellulose nanocrystal. *Mater Lett*. **2020**;*260*:126884.
41. Liu GF, Zhang D, Feng CL. Control of three-dimensional cell adhesion by the chirality of nanofibers in hydrogels. *Angew Chem Int Ed*. **2014**;*53*(30):7789–93.
42. Xu CY, Inai R, Kotaki M, Ramakrishna S. Aligned biodegradable nanofibrous structure: a potential scaffold for blood vessel engineering. *Biomaterials*. **2004**;*25*(5):877–86.
43. Kurpinski KT, Stephenson JT, Janairo RRR, Lee H, Li S. The effect of fiber alignment and heparin coating on cell infiltration into nanofibrous PLLA scaffolds. *Biomaterials*. **2010**;*31*(13):3536–42.